

A Numerical Model for Pore Pressure Buildup in a Porous Seabed under the Action of Combined Waves and Current

Yi-Fa Wang, Fu-Ping Gao

Key Laboratory for Mechanics in Fluid Solid Coupling Systems, Institute of Mechanics,
Chinese Academy of Sciences, Beijing, China

ABSTRACT

A finite element model for the pore pressure responses under the action of combined waves and current is proposed and verified with the existing experimental data. In this numerical model, both transient and residual pore pressure responses are simulated simultaneously. The numerical results indicate that the transient pore pressure is dominant in the upper part of the seabed while the residual component prevails in the lower one. Parametric studies are conducted to investigate the effects of the current velocity, the wave steepness, and the soil permeability on the pore pressure responses. Imposing a following or opposing current upon waves has much effect on pore pressure distributions in the porous seabed.

KEY WORDS: Residual pore pressure; liquefaction; combined waves and current; finite element modeling.

INTRODUCTION

While ocean waves propagating over the seabed in the shallow waters, the pore pressure could be generated in the seabed sediments. Two mechanisms of the wave-induced pore pressure responses have been recognized: one is the transient or oscillatory pore pressure accompanied by the damping of amplitude and phase lag in the pore pressure; the other is residual or progressive buildup of pore pressure caused by the cyclic shear stress within the seabed, which is similar to that induced by earthquakes. When the pore pressure in the seabed becomes excessive, the effective stress between the individual grains vanishes. Then soil liquefaction will occur, which may cause the instability of seabed and be a threat to the offshore structures. There are some failures of offshore structures because of soil liquefaction in the engineering practice (Christian et al., 1974; Zen et al., 1985; Lundgren et al., 1989). Thus, it is crucial for marine geotechnical engineers to adequately evaluate the pore pressure responses and soil liquefaction under the action of combined waves and current.

The transient mechanisms of wave-induced dynamic seabed responses have been investigated since the 1970s. Among these, Yamamoto et al. (1978) and Madsen (1978) derived analytical solutions of the wave-induced pore pressure, soil displacements and effective stresses in an infinite porous seabed based on Biot's consolidation theory (1941),

respectively. Mei and Foda (1981) proposed a simplified solution of wave-induced seabed responses with the boundary layer approximation. Hsu and Jeng (1994) further extended the analytical solutions to an unsaturated, isotropic seabed with finite thickness. Recently, Zhang et al. (2013) obtained an analytical solution for the wave-current induced soil responses in an infinite porous seabed using the third-order solution of wave-current interactions presented by Hsu et al. (2009). Numerous studies have been conducted to investigate the residual mechanisms of wave-induced pore pressure responses of the seabed. Seed and Rahman (1978) established a one-dimensional finite element model to describe the buildup of pore pressure under progressive waves with the empirical relationships obtained from cyclic triaxial or simple shear tests. Later, McDougal et al. (1989) solved the modified Biot's consolidation equation with a source term which governs the pore pressure generation and proposed a set of analytical solutions for the cases of shallow, finite and deep soil depths. Some similar investigations have been carried out by Cheng et al. (2001) and Jeng et al. (2007b). Jeng et al. (2007a) introduced an amplitude ratio to clarify the applicable ranges of the transient and residual mechanisms, considering the two components of the pore pressure separately. Li et al. (2011) coupled the two components and numerically investigated the pore pressure responses and soil liquefaction around a pile foundation under wave loading.

All the aforementioned studies, however, mainly focused on one of the mechanisms for the pore pressure responses individually or only considered the wave loading. In the offshore environments, the ocean waves always exist with current simultaneously and the wave-current induced transient and residual pore pressure responses are coupled actually, which may bring the seabed responses more complex than those under pure waves. However, the effects of current on the seabed responses are far from being well understood. Therefore, it is of interest to examine the pore pressure responses of a porous seabed under the action of combined waves and current.

In the present study, a FEM model is proposed to simulate both residual and transient pore pressure responses simultaneously under the action of combined waves and current. The numerical model is verified with the existing experimental data. Based on the numerical results, the effects of the current on the seabed responses are investigated. A parametric study is then carried out to investigate the effects of the magnitude of current velocity, the wave steepness, and the soil permeability on the transient and residual pore pressure responses.

NUMERICAL MODEL

The pore pressure responses under the action of combined waves and current are investigated numerically in this study, as illustrated in Fig. 1. The waves accompanied with a uniform current are assumed to propagate over an isotropic and homogeneous seabed along the positive x -direction, while the z -direction is upward from the interface between water and porous seabed.

Governing Equations

The governing equation for the pore-water flow within a porous seabed can be derived from Biot's consolidation equation with the assumption of compressible pore-water and soil-skeleton as:

$$\frac{k_s}{\gamma_w} \left(\frac{\partial^2 p}{\partial x^2} + \frac{\partial^2 p}{\partial z^2} \right) - \frac{n}{K'} \frac{\partial p}{\partial t} = \frac{\partial \varepsilon}{\partial t} \quad (1)$$

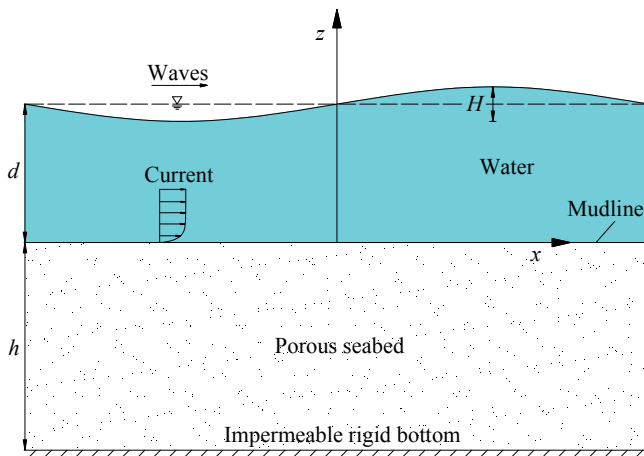


Fig. 1 Definition of wave-current-seabed interactions

where p is the pore-water pressure, k_s is the coefficient of soil permeability, γ_w is the unit weight of pore fluid, and n is the soil porosity. K' is the apparent bulk modulus of pore water, which is defined by:

$$\frac{1}{K'} = \frac{1}{K} + \frac{1-S_r}{p_{w0}} \quad (2)$$

where K is true bulk modulus of elasticity of water ($K = 2 \times 10^9 \text{ N/m}^2$), S_r is the degree of saturation, and p_{w0} is the absolute static pressure. In Eq. (1), ε is the volumetric strain, with volume reduction being considered positive. The analysis of Seed and Rahman (1978) relates the volume change to the dissipation of pore pressure from the soil skeleton, considering the pore pressure generation caused by the action of wave-induced cyclic shear stress under undrained conditions, i.e.

$$\frac{\partial \varepsilon}{\partial t} = m_v \left(\frac{\partial p}{\partial t} - \psi \right) \quad (3)$$

where ψ represents the rate of undrained pore pressure generation and can be written as $\psi = \partial u_g / \partial t$, in which u_g is the amount of pore pressure generation. For the linear elastic constitutive model under the

condition of plane strain, the coefficient of volume compressibility m_v can be expressed as:

$$m_v = \frac{1-2\nu}{G} \quad (4)$$

where G is shear modulus of the soil and ν is the Poisson's ratio. Substituting Eq. (3) into Eq. (1), renders the final form of the governing equation as:

$$\frac{\partial p}{\partial t} = \frac{1}{n/K' + m_v} \left(\frac{k_s}{\gamma_w} \nabla^2 p + m_v \psi \right) \quad (5)$$

To solve the governing equation Eq. (5), the amount of pore pressure generation u_g is required. Here it can be written as (Seed et al., 1976):

$$\frac{u_g}{\sigma_0} = \frac{2}{\pi} \arcsin \left(\frac{N}{N_1} \right)^{\frac{1}{2\theta}} \quad (6)$$

where σ_0 is the initial vertical effective stress, N is the number of cycles of shear stress at specified level, N_1 is the number of cycles to cause liquefaction, and θ is an empirical constant. Seed et al. (1976) suggested a typical value of $\theta = 0.7$ for an average condition. Rahman and Jaber (1986) examined the average condition and assumed a reasonable linear approximation which can be written as:

$$\frac{u_g}{\sigma_0} = \frac{N}{N_1} \quad (7)$$

The quantity σ_0 in Eqs. (6) and (7) is taken as the initial mean vertical effective stress:

$$\sigma_0 = -\frac{1+2K_0}{3} \gamma' z \quad (8)$$

where γ' is the submerged unit weight of the soil, and K_0 is the coefficient of lateral earth pressure. The quantity N_1 is a function of the cyclic shear stress ratio:

$$N_1 = \left(\frac{1-\tau}{\alpha \sigma_0} \right)^{\frac{1}{\beta}} \quad (9)$$

where α and β are the functions of the soil type and relative density, respectively (McDougal et al., 1989). τ represents the amplitude of the cyclic shear stress in the soil. In this numerical model, the analytical solution developed by Zhang et al. (2013) is adopted to determine the amplitude of the cyclic shear stress. The shear stress τ_{xz} obtained in their solution reads as follows:

$$\tau_{xz} = \sum_{m=1}^3 i P_m \left[(mkC_{0m} + (mkz - \lambda_m)C_{1m}) e^{mkz} + \delta_m C_{2m} e^{\delta_m z} \right] e^{im(kx - \omega t)} \quad (10)$$

where i is the imaginary unit, k is the wave number, and ω is the angular frequency of the wave. P_m ($m=1,2,3$) are parameters describing the dynamic wave pressure acting on the seabed, which related to the wave characteristics and the current velocity. C_{0m} , C_{1m} ,

C_{2m} , δ_m , and λ_m ($m=1,2,3$) are parameters closely related to the wave and current characteristics and soil properties. The details of the analytical expressions can be found in Zhang et al. (2013). It is noted that the shear stress in Eq. (10) is for the seabed of infinite thickness, hence the numerical model in this study is considered as the deep soil model (Jeng et al., 2007b), i.e. the soil depth in the range of $h/L > 0.3$, in which h is the seabed thickness and L is the wave length. It was demonstrated that the relative difference of pore pressure responses caused by infinite thickness for the deep soil model is rather small and could be neglected. Meanwhile, it is assumed that the buildup of pore pressure has slight effect on the shear stress, therefore the shear stress in Eq. (10) in which no accumulation of pore pressure tacks place can be approximately employed.

Initial and Boundary Conditions

To solve the governing equation Eq. (5), the initial and boundary conditions are applied as follows (see Fig. 2):

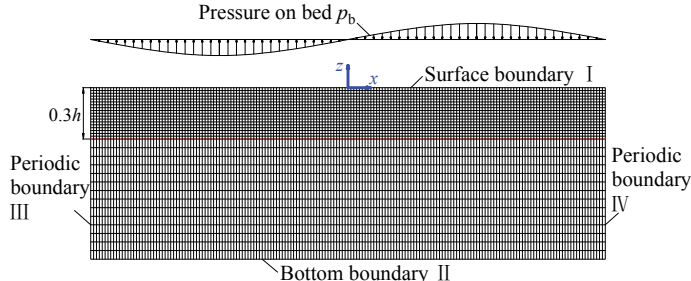


Fig. 2 Sketch of numerical model and FE mesh (not in scale)

Boundary I : the pore pressure is equal to the dynamic wave pressure induced by nonlinear waves and current loading along the surface of the seabed ($z = 0$), which can be expressed as:

$$p(x, z=0, t) = p_b(x, t) = P_m \cos[m(kx - \omega t)] \text{ at } z=0 \quad (11)$$

where P_m are the same as those described in Eq. (10). In the case of no current in the wave field, the above third-order solution can be reduced to the classic form of the solution of third-order nonlinear waves.

Boundary II : the bottom of the seabed is considered to be rigid and impermeable, hence there is no vertical flow at this bottom.

$$\frac{\partial p}{\partial z} = 0 \text{ at } z = -h \quad (12)$$

Boundary III, IV: the length of the computational domain is chosen to be equal to the wave length L . The periodic boundary condition is adopted according to the principle of repeatability (Zienkiewicz and Scott, 1972).

$$p|_{x=-\frac{L}{2}} = p|_{x=\frac{L}{2}} \quad (13)$$

The initial condition is set as:

$$p(x, z, 0) = 0 \quad (14)$$

Fig. 2 shows the computational domain of the numerical model and the finite element mesh used in this study. Quadratic Lagrange elements are used in the present finite-element model. It was emphasized by Cheng

et al. (2001) that the pore pressure buildup for deep soil conditions is more sensitive to the shear stress near the seabed. Therefore, more and finer meshes are adopted near the seabed surface (i.e. the upper soil depth of $|z|/h < 0.3$ near the mudline) to ensure high accuracy of numerical solution. A time step of $0.1T$ is applied to sufficiently handle the computational time and properly simulate the pore pressure responses under combined waves and current, here T is the wave period.

Verification of Numerical Model

In this study, the proposed numerical model is verified with the existing experimental data. Since the experimental investigation on the seabed responses under combined waves and current is quite scarce up to now and almost limited to wave loading only, the present numerical model will be reduced to the case without current. The experiment data conducted by Sumer et al. (2012) is employed.

Sumer et al. (2012) conducted a series of experiments in a wave flume to obtain data of buildup of pore pressure under waves. The pore pressure in the middle of the soil pit at five depths was measured with miniature pore pressure transducers. The test soil used in the experiments was silt with the mean size of soil grains $d_{50} = 0.070$ mm.

The soil properties are provided as follows: $G = 2 \times 10^6$ N/m² , $k_s = 1.5 \times 10^{-5}$ m/s , $\gamma' = 8.13 \times 10^3$ N/m³ , $\nu = 0.29$, $n = 0.51$, $S_r = 1$, $K_0 = 0.42$, $\alpha = 0.20$, $\beta = -0.45$, $h = 0.4$ m . The wave characteristics of the regular waves are as follows: the water depth $d = 0.55$ m , the wave height $H = 0.18$ m , the wave period $T = 1.6$ s .

For comparison, wave and soil parameters used in the numerical model are consistent with those in the experiments. It is noted that the measured pore pressure provided by Sumer et al. (2012) is the residual period-averaged pore water pressure, which can be expressed as:

$$\bar{p} = \frac{1}{T} \int_t^{t+T} pdt \quad (15)$$

However, the present numerical model simulates both components of transient and residual pore pressure, thus the residual period-averaged pore pressure is calculated and extracted from Eq. (15) for comparison.

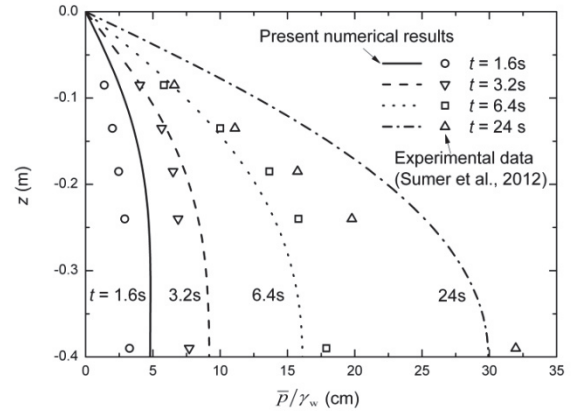


Fig. 3 Comparisons of the time development of wave-induced residual period-averaged pore pressures between the present numerical results and the experimental data

Fig. 3 compares the vertical distributions of the residual period-averaged pore pressure from the numerical model and the experimental

data at four different time. It is indicated that the numerical results predicted by the present numerical model overall agree well with the experimental data.

RESULTS AND DISCUSSIONS

Time-dependent Pore Pressure Responses under Combined Nonlinear Waves and Current

When the seabed is under the loading of combined nonlinear waves and current, the numerical results indicate that the pore pressure in the soil fluctuates while accumulating to the equilibrium state (i.e. the residual period-averaged pore pressure gets the maximum value) gradually (see Fig. 4). Numerical examples illustrate the time-history of pore pressure development and show when the pore pressure reaches the equilibrium state. The input data for numerical examples are tabulated in Table 1. In the numerical examples, a positive current velocity represents the current and waves being the same direction (i.e. the following current), while the negative value denotes the current and waves being an opposite direction (i.e. the opposing current).

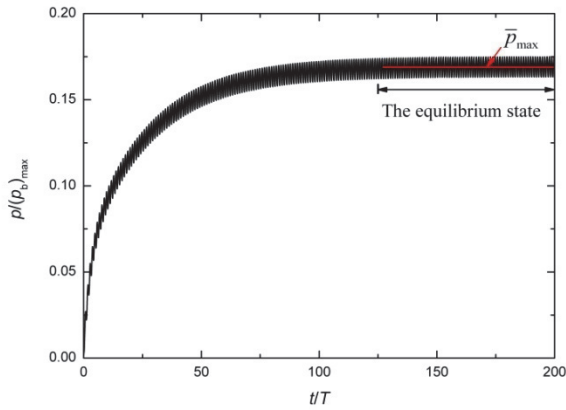


Fig. 4 Time development of pore pressure buildup under the action of combined waves ($H = 5.0 \text{ m}$, $T = 8.0 \text{ s}$) and a following current ($U_c = 1.0 \text{ m/s}$) in the soil at $z = -10 \text{ m}$, $x = 0$.

Table 1. Input data for numerical examples

Wave and Current Characteristics

Wave period T	8.0 s
Water depth d	10.0 m
Wave height H	5.0 m (various)
Current velocity U_c	1.0 m/s (various)
Wave length L	88.2 m (various)
<i>Soil Properties</i>	
Seabed thickness h	30.0 m
Poisson's ratio ν	0.35
Soil porosity n	0.46
Shear modulus G	$1.0 \times 10^7 \text{ N/m}^2$
Coefficient of permeability k_s	$5.0 \times 10^{-4} \text{ m/s}$ (various)
Unit weight of pore water γ_w	$9.8 \times 10^3 \text{ N/m}^3$
Submerged unit weight of soil γ'	$10.7 \times 10^3 \text{ N/m}^3$
Degree of saturation S_r	1.0
Coefficient of lateral earth pressure K_0	0.40
α	0.246
β	-0.165

Fig. 5 presents the vertical distributions of time-dependent pore pressure responses under waves and the following current ($U_c = 1.0 \text{ m/s}$) loading along $x = 0$ (i.e. the midline of the computational domain). In Fig. 5, the pore pressure variables are normalized by the maximum dynamic wave pressure along the seabed surface. Here five different characteristic time of an integer wave period while the wave crests passing the midline of the computational domain is chosen to analyze the pore pressure development. It is seen from Fig. 5 that the pore pressure attenuates significantly in the upper thin part of the seabed, which may be due to the damping of amplitude and phase lag for the transient pore pressure within the seabed. The transient component of pore pressure which is independent of time dominates in the upper part of the seabed. Meanwhile, the residual pore pressure is initially built up in the upper part of the soil near the mudline and then propagates towards the impermeable bottom for the deep soil model, which is dominant in the lower part of the seabed. In this case study as shown in Fig. 5, the cyclic pore pressure is developing gradually and approaching an equilibrium state at approximately $100T$ (i.e., about 100 times of cyclic loading). It is noted that the time needed to reach the equilibrium state varies with the waves/current characteristics and the soil properties. The pore pressure responses of the entire computational domain normalized by the maximum dynamic wave pressure along the mudline at $t = 200T$ are plotted in Fig. 6. For the soil depth $|z|/h > 0.4$ (see Fig. 5 & 6), the pore pressure remains almost identical, indicating the finite thickness of the seabed has slight effect on the pore pressure distribution for the deep soil model.

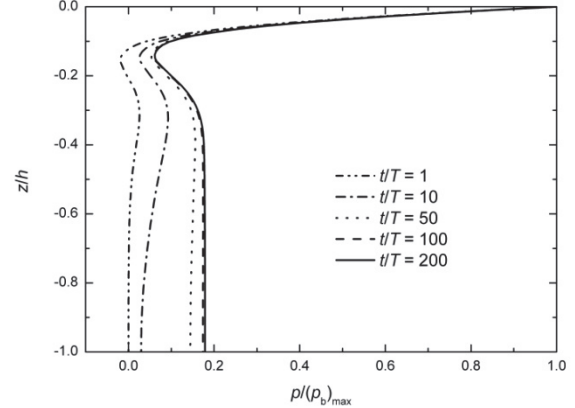


Fig. 5 Distributions of the time-dependent pore pressure along the soil depth at $x = 0$ ($U_c = 1.0 \text{ m/s}$, $H = 5.0 \text{ m}$, $T = 8.0 \text{ s}$)

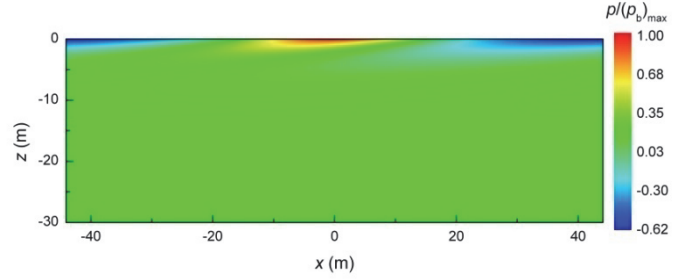


Fig. 6 Distributions of the excess pore pressure in the entire computational domain at $t = 200T$ ($U_c = 1.0 \text{ m/s}$, $H = 5.0 \text{ m}$, $T = 8.0 \text{ s}$)

Parametric Study

A parametric study is carried out to examine the influences of three parameters: the magnitude of current velocity, the wave steepness and the coefficient of permeability on both transient and residual pore pressure responses under the action of combined waves and current. The input data for the parametric study remain the same as given in Table 1.

Effects of Imposing a Following or Opposing Current

The primary objective is to examine the effects of imposing a current upon waves on pore pressure responses, hence the following current and opposing current with various magnitudes of velocity are investigated and the case without current (i.e. only third-order nonlinear waves are considered) are included for the purpose of comparisons.

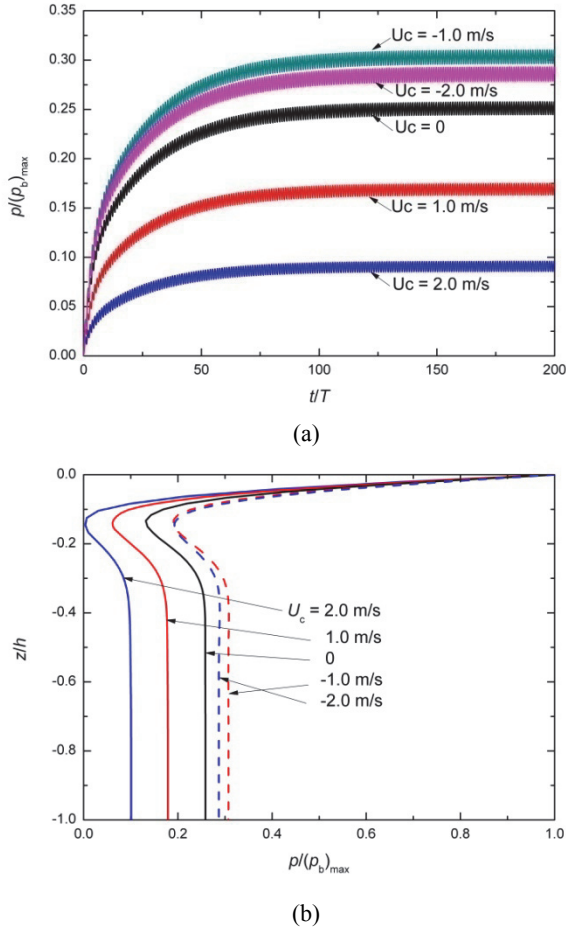


Fig. 7 The pore pressure response for various magnitudes of current velocity: (a) time developments of pore pressure at $z = -10$ m, $x = 0$; (b) vertical distributions of pore pressure along $x = 0$ ($H = 5.0$ m, $k_s = 5.0 \times 10^{-4}$ m/s)

Fig. 7 presents the time developments of pore pressure at $z = -10$ m, $x = 0$ and the vertical distributions of pore pressure along $x = 0$ with different values of the magnitude of current velocity U_c . As shown in Fig. 7a, the amplitude of transient pore pressure is somewhat reduced for the following current, while enlarged for the opposing current. The residual pore pressure accumulates to a larger value for the opposing current than that of the following current and wave only

conditions. Fig. 7b illustrates the vertical distributions of pore pressure along $x = 0$. All of them correspond to the time when the pore pressure reaches the equilibrium state and the wave crest pass the midline of the computational domain. It can be seen that the attenuation of pore pressure in the upper part of the seabed is slightly greater for larger current velocity. Furthermore, the pore pressure in the lower part of the seabed where dominating by the component of residual pore pressure, is sensitive to the current velocity and becomes larger for the condition of imposing an opposing current than the condition of pure waves (no current).

Effects of Wave Steepness

Wave steepness is one of the main wave parameters that should be considered in the analysis of seabed responses. Here the cases of non-breaking waves are investigated, in which the maximum wave steepness satisfies:

$$\left(\frac{H}{L}\right)_{\max} \leq 0.142 \tanh\left(\frac{2\pi d}{L}\right) \text{ and } \left(\frac{H}{d}\right) \leq 0.78 \quad (16)$$

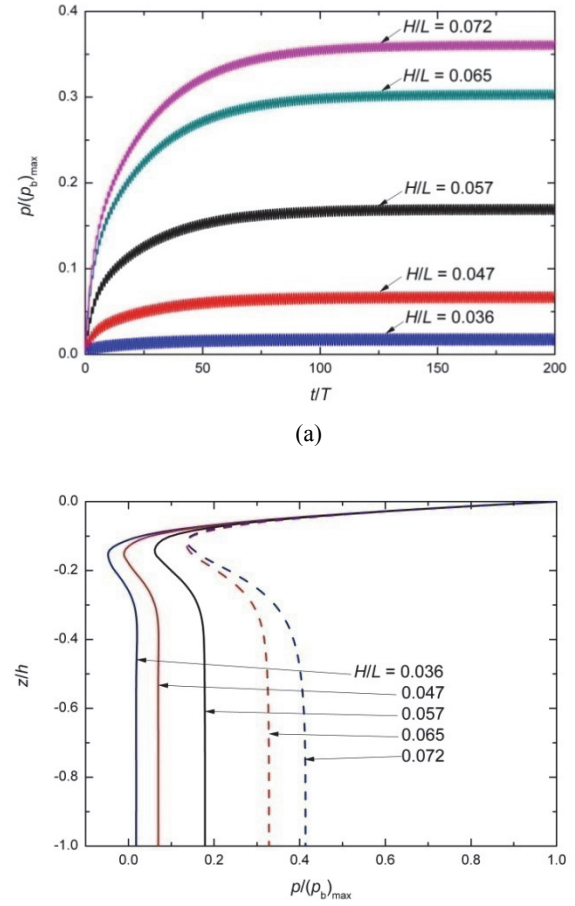
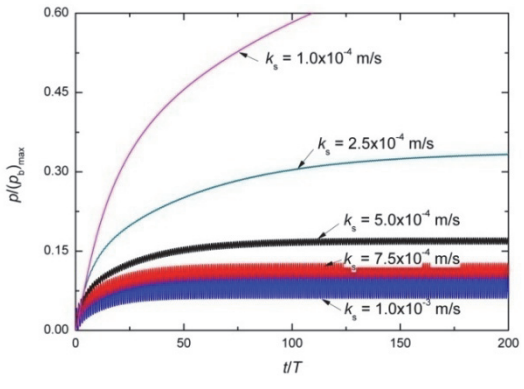


Fig. 8 The pore pressure response for various values of wave steepness: (a) time developments of pore pressure at $z = -10$ m, $x = 0$; (b) vertical distributions of pore pressure along $x = 0$ ($k_s = 5.0 \times 10^{-4}$ m/s, $U_c = 1.0$ m/s)

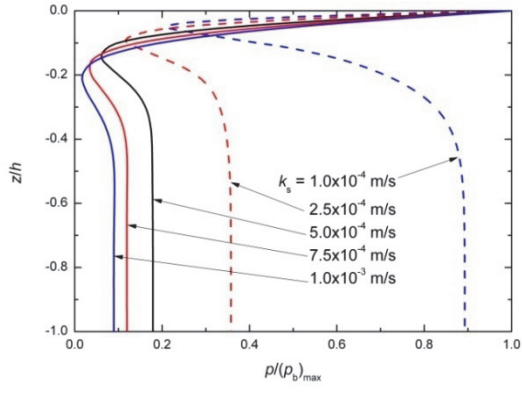
Fig. 8 illustrates the time developments of pore pressure at $z = -10 \text{ m}$, $x = 0$ and the vertical distributions of pore pressure along $x = 0$ with different values of wave steepness H/L . It can be seen from Fig. 8a that the wave steepness has significant effect on the buildup of pore pressure, increasing with the increase of wave steepness. However, the transient component of pore pressure is not very sensitive to the wave steepness. Fig. 8b shows the vertical distributions of pore pressure along $x = 0$ at the moment when the pore pressure reaches the equilibrium state. It is indicated that the larger wave steepness, the larger the pore pressure accumulates in the lower part of the seabed, while there is little differences for the attenuation of pore pressure in the upper part with variations of wave steepness.

Effects of Soil Permeability

Soil permeability is a dominant parameter in evaluating the waves and current induced soil responses.



(a)



(b)

Fig. 9 The pore pressure response for various values of soil permeability: (a) time developments of pore pressure at $z = -10 \text{ m}$, $x = 0$; (b) vertical distributions of pore pressure along $x = 0$ ($U_c = 1.0 \text{ m/s}$, $H = 5.0 \text{ m}$)

Fig. 9 shows the time developments of pore pressure at $z = -10 \text{ m}$, $x = 0$ and the vertical distributions of pore pressure along $x = 0$ with different values of the coefficient of permeability k_s . As shown in Fig. 9a, for $k_s = 1.0 \times 10^{-3} \text{ m/s}$, the residual pore pressure is negligible compared with the transient pore pressure. On the other hand, for $k_s = 1.0 \times 10^{-4} \text{ m/s}$, the buildup of pore pressure prevails and gets

more obvious. It is indicated that the pore pressure accumulates larger under smaller soil permeability, while it will take longer to build up to the equilibrium state. Fig. 9b illustrates the vertical distributions of pore pressure along $x = 0$ at the moment when the pore pressure reaches the equilibrium state. It is shown that the rate of the pore pressure attenuation is more obvious for smaller soil permeability, while the pore pressure in the lower part of the seabed increases with the decrease of soil permeability.

CONCLUSIONS

A finite element model is proposed to simulate both residual and transient pore pressure responses simultaneously under the action of combined waves and current. The numerical model is verified with the existing experimental data and an overall agreement is found. Based on the numerical results, the following conclusions can be drawn.

The pore pressure attenuates remarkably in the upper part of the seabed where dominated by the transient component, while accumulating to the equilibrium state gradually under the combined nonlinear waves and current. The residual component of pore pressure is dominant in the deep depth of the seabed and almost keeps identical below a certain depth.

The parametric study indicates that under combined nonlinear waves and current, the pore pressure buildup in the porous seabed is affected by the wave steepness, the imposed current velocity and the soil permeability, etc.

ACKNOWLEDGEMENTS

This work is financially supported by the Major State Basic Research Development Program of China ("973" Program) (Grant No. 2014CB046204) and National Natural Science Foundation of China (Grant Nos. 11232012).

REFERENCES

- Biot, M.A. (1941). "General theory of three-dimensional consolidation," *Journal of Applied Physics*, Vol 12, No 2, pp 155-64.
- Cheng, L., Sumer, B.M. and Fredsoe, J. (2001). "Solutions of pore pressure build up due to progressive waves," *International Journal for Numerical and Analytical Methods in Geomechanics*, Vol 25, No 9, pp 885-907.
- Christian, J.T., Taylor, P.K., Yen, J.K.C. and Erali, D.R., (1974). Large diameter underwater pipe line for nuclear power plant designed against soil liquefaction. *Proceeding of the Annual Offshore Technology Conference*, Houston, pp 597-606.
- Hsu, H.C., Chen, Y.Y., Hsu, J.R.C. and Tseng, W.J. (2009). "Nonlinear water waves on uniform current in lagrangian coordinates," *Journal of Nonlinear Mathematical Physics*, Vol 16, No 1, pp 47-61.
- Jeng, D.S., Seymour, B., Gao, F.P. and Wu, Y.X. (2007a). "Ocean waves propagating over a porous seabed: Residual and oscillatory mechanisms," *Science China Ser. E-Technological Sciences*, Vol 50, No 1, pp 81-89.
- Jeng, D.S., Seymour, B.R. and Li, J. (2007b). "A new approximation for pore pressure accumulation in marine sediment due to water waves," *International Journal for Numerical and Analytical Methods in Geomechanics*, Vol 31, No 1, pp 53-69.
- Li, X.J., Gao, F.P., Yang, B. and Zang, J. (2011). "Wave-induced pore pressure responses and soil liquefaction around pile foundation," *International Journal of Offshore and Polar Engineering*, ISOPE, Vol 21, No 3, pp 233-239.
- Lundgren, H., Lindhardt, J.H.C. and Romhild, C.J., 1989. Stability of breakwaters on porous foundation. *Proceedings of 12th International Conference on Soil Mechanics and Foundation Engineering*, pp 451-

- Madsen, O.S. (1978). "Wave-induced pore pressures and effective stresses in a porous bed," *Geotechnique*, Vol 28, No 4, pp 377-393.
- McDougal, W.G., Liu, P.L.F., Clukey, E.C. and Tsai, Y.T. (1989). "Wave-induced pore water pressure accumulation in marine soils," *Journal of Offshore Mech Arctic Engineering*, Vol 111, No 1, pp 1-11.
- Mei, C.C. and Foda, M.A. (1981). "Wave-induced responses in a fluid-filled poro-elastic solid with a free-surface - a boundary-layer theory," *Geophysical Journal of the Royal Astronomical Society*, Vol 66, No 3, pp 597-631.
- Rahman, M.S. and Jaber, W.Y. (1986). "A simplified drained analysis for wave-induced liquefaction in ocean floor sands," *Soils and Foundations*, Vol 26, No 3, pp 57-68.
- Seed, H.B., Lysmer, J. and Martin, P.P. (1976). "Pore-water pressure changes during soil liquefaction," *Journal of Geotechnical Engineering Division, ASCE*, Vol 102, No 4, pp 323-346.
- Seed, H.B. and Rahman, M.S. (1978). "Wave-induced pore pressure in relation to ocean-floor stability of cohesionless soils," *Marine Geotechnology*, Vol 3, No 2, pp 123-150.
- Sumer, B.M., Kirca, V.S.O. and Fredsoe, J. (2012). "Experimental validation of a mathematical model for seabed liquefaction under waves," *Int. J. Offshore Polar Eng.*, Vol 22, No 2, pp 133-141.
- Yamamoto, T., Koning, H.L., Sellmeijer, H. and Hijum, E.V. (1978). "On the response of a poro-elastic bed to water waves," *Journal of Fluid Mechanics*, Vol 87, No 1, pp 193-206.
- Zen, K., Umehara, Y. and Finn, W.D.L., (1985). A case study of the wave-induced liquefaction of sand layers under damaged breakwater. *Proceedings 3rd Canadian Conference on Marine Geotechnical Engineering*, pp 505-520.
- Zhang, Y., Jeng, D.S., Gao, F.P. and Zhang, J.S. (2013). "An analytical solution for response of a porous seabed to combined wave and current loading," *Ocean Engineering*, Vol 57, No 1, pp 240-247.
- Zienkiewicz, O.C. and Scott, F.C. (1972). "On the principle of repeatability and its application in analysis of turbine and pump impellers," *International Journal for Numerical Methods in Engineering*, Vol 4, No 3, pp 445-448.